Numerical Simulation of Liquid Phase Diffusion Growth of SiGe Single Crystals under Zero Gravity

M. Sekhon[1], N. Armour[1], S. Dost[1,2]

Abstract: Liquid Phase Diffusion (LPD) growth of Si_xGe_{1-x} single crystals has been numerically simulated under zero gravity. The objective was to examine growth rate and silicon concentration distribution in the LPD grown crystals under diffusion dominated mass transport prior to the planned LPD space experiments on the International Space Station (ISS). Since we are interested in predicting growth rate and crystal composition, the gravitational fluctuation of the ISS (g-jitter) was neglected and the gravity level was taken as zero for simplicity.

A fixed grid approach has been utilized for the simulation. An integrated top-level solver was developed in OpenFOAM to carry out numerical simulations for the melting and solidification periods of the LPD growth process. The solver employs the well-known enthalpy method for modeling the initial melting process and uses the virtual front-tracking method, originally developed to model dendritic growth. This simulates the solidification as driven by saturation and precipitation as is the case for this solution growth technique. The melting simulation determines the initial conditions for growth interface, temperature, and concentration. The solver then calculates the onset of solidification, the evolution of the growth interface. In addition, the concentration and temperature fields are calculated in the melt and grown crystal.

The present simulation results agree qualitatively with the radial and axial silicon distributions in the grown crystals of the Earth-bound experiments, and also with those previously predicted numerically. The computed total growth rate also agrees quantitatively with that of the experiment. However, the simulation shows slight differences in the interface shapes and predicts faster initial growth rate. Such a small discrepancy is expected since the contribution of natural convection in the melt was not included in the present simulation. A well-design LPD space experiment may shed light on this prediction.

[1] Crystal Growth Laboratory, Department of Mechanical Engineering, University of Victoria, Victoria, BC Canada V8W3P6.

[2] Corresponding author: sdost@me.uvic.ca

Keywords: Fixed grid; Enthalpy method; Modeling; Simulation; Crystal growth; Solidification; Silicon; Germanium

1   Introduction

Si_xGe_{1-x} is an alloy semiconductor material possessing a complete solid and liquid miscibility, making it an attractive choice for both epitaxial and bulk crystal growth processes. Its properties can be adjusted for the needs of a variety of applications [Kasper (1995), Yonenaga (2005)]. Various melt growth techniques have been used to grow bulk single crystals of Si_xGe_{1-x} [see for instance the review article of Schilz and Romanenko (1995), and also Yonenaga et al. (1995), Wollweber et al. (1996a,b), Abrosimov et al. (1996, 1997), Dold et al. (1998), Campbell et al. (2001), Volz et al. (2002), Usami (2011)]. However, growing bulk Si_xGe_{1-x}single crystals of uniform composition by the melt growth techniques is still a challenge. This is primarily due to the large miscibility gap in the silicon germanium phase diagram that requires silicon be replenished during melt growth [Abrosimov et al. (1997) and Usami (2011)].

Liquid Phase Diffusion (LPD) is a solution growth technique that was originally developed by Nakajima et al. (1999) as a variant of multicomponent zone melting growth [Nakajima et al. (1996), and Suzuki et al. (1996)], who utilized it to grow bulk Si_xGe_{1-x} crystals with an initial graded composition region (from $x = 0$ to $x = 0.02$) followed by a uniform region at $x = 0.02$. This technique was then utilized by Yildiz et al. (2005) to grow graded bulk crystals from the germanium side with the main objective of production of seed crystals for successive crystal growth techniques, such as Czochralski and Liquid Phase Electroepitaxy (LPEE). Further research has been carried out on SiGe growth by LPD by Armour and Dost (2010a,b,c) where the effects of rotating and static magnetic fields on the transport process were investigated.

LPD growth is based on the principle of saturation and precipitation like all solution growth techniques. This differs from melt growth where solidification is achieved by cooling the melt below its melting point. A schematic description of the LPD growth crucible is given in Figure 1. The growth cell consists of a Germanium single crystal seed at the bottom, Silicon source material at the top and polycrystalline Germanium solvent material sandwiched in the middle. This configuration is subjected to an axial temperature gradient such that the Germanium solvent material melts completely and the Germanium seed only partially melts back. The extent of melt back establishes the initial growth interface. The source material (Si) remains solid because of its higher melting point. The area of contact between the silicon source and the Si-Ge solution (initially pure Ge) forms the dissolution interface. The dissolved Si is primarily transported through the solution, towards the growth
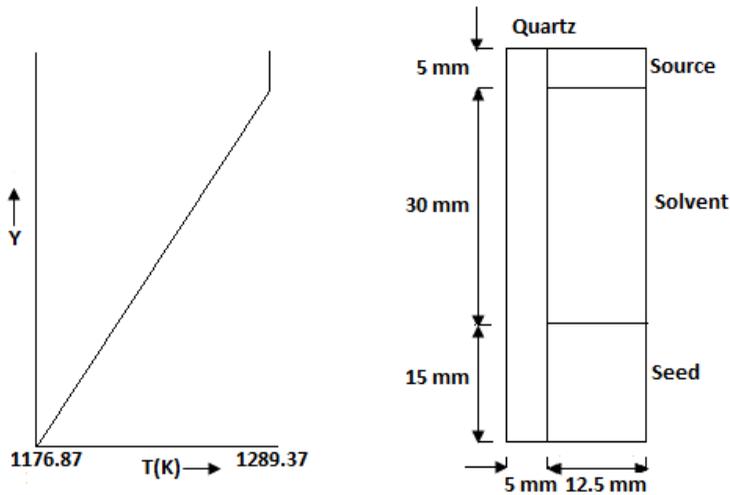
Figure 1: Schematic diagram of the LPD growth system: applied temperature profile on left, and half of the crucible domain on right.

interface, by diffusion. The phase diagram governs the solubility of silicon in the germanium melt. The solubility of the silicon changes throughout the melt due to the applied temperature gradient. The temperature in the immediate vicinity of the growth interface is the lowest, and accordingly the solubility is the lowest in this region. Silicon is incorporated into the melt at the dissolution interface at a higher concentration, due to the higher temperature at that point. With transport of silicon from the dissolution to growth interface, the solubility limit of the silicon around the growth interface is exceeded and growth occurs. A SiGe crystal with a graded Si composition from the Ge side is produced. The growth continues with time with increasing Si composition until the process is terminated.

In terms of modeling, bulk crystal growth consists of various processes occurring at scales varying from microscopic to macroscopic. This makes the development of a comprehensive model almost impossible as clearly pointed out by Yeckel and Derby (2005). Based on the model objectives, models can be classified as process models or defect models where crystal defects are related to process conditions [Muller and Friedrich (2004)]. Global or overall models, as termed in the literature, refer to a modeling approach in which the furnace is also part of the computational domain rather than using boundary conditions on the growth crucible to account for the effect of the furnace [Van den Bogaert and Dupret (1997)]. Although significant

progress has been made in modeling of transport phenomena in crystal growth, it still continues to be a challenge due to the various complexities involved. In particular, the handling of the moving interface inherent in most growth processes continues to be difficult [Fischer et al. (2005)].

There are various numerical techniques for handling a moving boundary problem. These techniques fall into two main groups: i) Lagrangian methods that utilize an interface adjusting moving grid, and ii) Eulerian techniques that are based on a fixed grid approach and the interface position is obtained as part of solution [Shyy et al. (1996)]. While each of these two approaches has its own advantages and disadvantages, the important advantage of the fixed grid approach lies in its relative simplicity. The basic approach is to represent the entire domain by a single set of field equations. Detailed derivation of these equations using the continuum mixture theory for solidification/melting problems can be found in Bennon and Incropera (1987). The enthalpy-porosity technique, given by Voller and Prakash (1987), is based on the fixed grid approach and has been successfully used to simulate various melt growth techniques [see for instance Ouyang and Shyy (1996, 1997), Jarvinen et al. (1997), Morvan et al. (1999), Martinez-Tomas and Munoz (2001), El Ganaoui et al. (2002) and Nikrityuk et al. (2012)].

Yildiz et al. (2005) and Yildiz and Dost (2005) developed a numerical simulation model to predict experimental results in which the moving grid approach was employed and the effect of natural convection was included. Simulations shed light on the LPD process and showed close agreement with experiments. The combined effects of static and rotating magnetic fields in this growth system was also studied numerically by Yildiz et al. (2006) and Yildiz and Dost (2007).

In the present work, we were interested only in growth rate (the evolution of the growth interface) and silicon concentration in the grown crystals under microgravity conditions. Thus the effect of fluid flow in the melt under the microgravity level (about 10^{-4}g to 10^{-5}g) of the ISS is neglected by taking the gravity level as zero (diffusion driven transport). We have also neglected the gravity fluctuation (g-jitter) of the ISS in the simulation since mass transport is usually not so responsive to the g-jitter of the ISS [Okano et al. (2001), (2003) and (2006), and Takagi (2012)].

We have selected the fixed grid approach. This was motivated by the simplicity and widespread usage of the approach in obtaining numerical solutions of solidification problems [Shyy et al. (1996)]. This also allowed us to carry out simulation for a longer duration (up to 132 h). Section 2 describes the model equations used to simulate the melting and solidification processes. A brief discussion of the solution algorithm and numerical solution procedure is given in Sections 3 and 4. The simulation results are presented in Section 5. Results are compared with the Earth-bound LPD experiments and also with those earlier numerical simulation results.

2 Model description

From a numerical simulation point of view, the LPD growth process consists of two main stages: the melting period and the following solidification process. During melting, the Ge molten section (melt) and the initial growth and dissolution interfaces form. Models used for simulating each of these two stages are presented below.

2.1 Modeling the melting of germanium

The well-known enthalpy-porosity method given by Voller and Prakash (1987) was used to model the melting of pure germanium. In this method, a single set of field equations is used to model the entire domain (molten and solid). The interface is computed as part of the solution rather than tracking it explicitly. To account for the absorption of latent heat during melting, a sink term is added to the energy equation. Depending upon the manner in which liquid fraction is updated after each time step there are two variants of this method called the T-based and H-based methods [Shyy et al. (1996)]. In the T-based method, liquid fraction for each cell is updated based on its temperature but the update expression assumes that a phase change occurs over a range of temperatures, which is not realistic for the phase change of pure components. The H-based method uses an inverted enthalpy-temperature relationship, i.e. it uses $T = T(H)$ rather than $H = H(T)$. Since temperature is a continuous function of enthalpy for the phase change process, this approach eliminates the need to make the assumption that phase change occurs over a range of temperature, and is well suited for modeling an isothermal phase change. The H-based method was utilized in the model presented.

2.2 Modeling the solidification of Si_xGe_{1-x} single crystal

As described earlier, solidification in the LPD process occurs due to saturation and precipitation. The use of the conventional enthalpy method is not appropriate as it is not well suited to model solidification processes that are not driven by cooling the melt. However, it is possible to model the LPD process using a virtual front tracking model, as given by Zhu and Stefanescu (2007). This approach was developed for modeling dendritic growth where the solidification process also occurs due to saturation and precipitation. This approach was utilized in the present work since the contribution of natural convection was not included.

In the present model, solidification in a computational cell is predicted when concentration in the cell exceeds the equilibrium concentration of silicon, as computed from the phase diagram using the local temperature. The release of latent heat during solidification is accounted for by including a sink term in the energy equation.

The solidification of SiGe causes the melt in the region of growth to deplete in silicon due to the miscibility gap in the phase diagram. This decrease of silicon concentration in the melt as solidification proceeds is accounted for by including a sink term in the mass transport equation.

2.2.1   Assumptions

In the modeling we have made the following assumptions.

- Effect of natural convection in the Si-Ge melt (solution) is neglected since we consider zero gravity.

- Enthalpy of mixing associated with the dissolution of silicon into the Si-Ge melt is neglected as silicon and germanium form a nearly ideal solution.

- Local thermodynamic equilibrium is assumed at the dissolution and growth interfaces.

- Dissolution interface is considered to be stationary since its velocity (silicon dissolution rate) is very small in comparison to the growth velocity.

- The Si-Ge solution (melt) is assumed to be dilute in silicon concentration.

- Classical Fourier's law of heat flux and Fick's law of mass flux are used. Soret and Dufour effects were not taken into account.

- The coefficients of thermal and mass diffusivities are assumed to remain constant.

- The mass diffusivity of silicon in solid germanium is small compared to that in the germanium melt and is not taken into account.

- The system is considered to be axisymmetric and remains axisymmetric during growth.

- The solid and liquid densities are assumed to be equal.

2.3   Numerical solution domain

The numerical solution domain consists of the solid Ge seed at the bottom, Si-Ge solution (initially pure Ge melt) in the middle, the Si solid source at the top, and the wall of the quartz ampoule. The domain and the applied temperature profile are shown in Figure 1. For the simulation The OpenFOAM solver was used with

the "conjugate heat foam" base solver supplied with "OpenFoam-1.6ext". However, in the top-level code a number of changes were made including a) extending the solver to three subdomains (melt, quartz, and source), b) implementing the enthalpy-porosity technique, and c) implementing solidification.

The OpenFOAM solver utilized always uses the three-dimensional Cartesian coordinate system. To simulate a two-dimensional axisymmetric system the geometry was specified as wedge with a small angle ($<5^0$) (OpenCFD (2013) and Weller et al. (1998)). To keep the interface thickness small, a fine mesh was employed in the melt region (10 mesh elements per mm) whereas a relatively coarser mesh was used for the source and quartz regions (5 mesh elements per mm) for computational efficiency.

2.4   Field equations

Two different sets of field equations (energy and mass transport) were solved corresponding to the melting and solidification models. The energy equation was solved for the entire domain and the mass transport equation was only solved for the melt region.

2.4.1   Melting

In the melt, only the energy balance and mass transport equations are solved as the contribution of fluid flow was neglected. The energy balance yields the following equation:

$$\frac{\partial T}{\partial t} = \alpha \nabla^2 T - S_T \tag{1}$$

where ∇^2 is the two-dimensional gradient operator, and α is the thermal diffusivity with different values in the liquid and solid phases.

$$\alpha = \begin{cases} \alpha_s & \text{if} \quad \varepsilon < 1 \\ \alpha_l & \text{if} \quad \varepsilon = 1 \end{cases} \tag{2}$$

The last term in Eq. (1) is the sink term representing the contribution of latent heat and is defined by:

$$S_T \equiv \frac{L}{c_p} \frac{\partial \varepsilon}{\partial t} \tag{3}$$

Mass transport equation reduces to:

$$\frac{\partial C}{\partial t} = D \nabla^2 C \tag{4}$$

where D is the diffusion coefficient with different values in the solid and liquid phases:

$$D = \begin{cases} D_s & \text{if} \quad \varepsilon < 1 \\ D_l & \text{if} \quad \varepsilon = 1 \end{cases} \tag{5}$$

The enthalpies are defined by

$$H_p^n = C_p T_p^{(n-1)} + \varepsilon^{(n+1)} L \quad \text{and} \quad \varepsilon^n = \begin{cases} 0 & \text{if} \quad H_p^n < H_s \\ \frac{H_p^n - H_s}{H_l - H_s} & \text{if} \quad H_s \leq H_p^n \leq H_l \\ 1 & \text{if} \quad H_p^n > H_l \end{cases} \tag{6}$$

2.4.2   Solidification

In solidification the energy balance and mass transport equations in the melt are reduced to:

$$\frac{\partial T}{\partial t} = \alpha \nabla^2 T + S_T' \quad \text{and} \quad \frac{\partial C}{\partial t} = D \nabla^2 C + S_C \tag{7}$$

where the corresponding source terms are defined as

$$S_T' \equiv \frac{L}{c_p} \frac{\partial \gamma}{\partial t} \quad \text{and} \quad S_C \equiv C(1 - K) \frac{\partial \gamma}{\partial t} \tag{8}$$

with

$$\alpha = \begin{cases} \alpha_l \, if \, \gamma < 1 \\ \alpha_s \, if \, \gamma = 1 \end{cases} \quad \text{and} \quad D = \begin{cases} D_l \, if \, \gamma < 1 \\ D_s \, if \, \gamma = 1 \end{cases} \tag{9}$$

and

$$\Delta\gamma_{lever}^N = \frac{C^{N-1} - C_l^{N-1}}{C_s^{N-1} - C_l^{N-1}}, \quad \Delta\gamma^N = min(\Delta\gamma_{lever}^N, 1 - \sum_{N=1}^{N_T - 1} \Delta\gamma_{lever}^N),$$
$$\gamma^N = \sum_{N=1}^{N} \Delta\gamma^N, \quad \text{and} \quad \gamma^{N_T} = \sum_{N=1}^{N_T} \Delta\gamma^N = 1 \tag{10}$$

2.4.3   Quartz wall and solid source

In both melting and solidification, we only have the heat conduction equation with appropriate thermal diffusivity coefficients:

$$\frac{\partial T}{\partial t} = \alpha \nabla^2 T \tag{11}$$

3   Solution algorithm

3.1   Melting solver

The melting solver utilizes the *H*-based enthalpy-porosity method (Shyy et al. (1996)) and the solidification solver uses the algorithm proposed by Zhu and Stefanescu (2007). The steps are as follows:

1. Initialize the concentration field, and set the liquid fraction to zero in the melt sub-domain (seed and solvent region) and the temperature field to 298K in the entire domain. Also, initialize thermal diffusivity to an appropriate value in each sub-domain.

2. Based on the previous time step values of temperature and liquid fraction, update the enthalpy of each cell using Eq.$(6)_1$.

3. Compute the liquid fraction for each cell using Eq.$(6)_2$.

4. Update diffusion coefficient and thermal diffusivity for each cell (Eqs. (2) and (5)) and compute the sink term for energy equation (Eq. (3)) which is dependent upon the rate of change of liquid fraction.

5. Solve energy and mass transport equations (Eqs. (1) and (4)).

6. If the melting process is complete, switch to solidification solver or else go to step b.

3.2   Solidification solver

1. Initialize concentration and temperature fields to the values obtained from melting solver and also identify the remaining solid seed region in the melt sub-domain. Set the solid fraction to unity in the solid seed region and to zero in the remaining melt subdomain.

2. Check the state of each cell in the melt region. If it lies in the solid seed region or if it is a fully solidified cell ($\gamma = 1$) then it does not enter the solidification loop. For other cells in melt region (i.e. $\gamma < 1$) proceed to step c.

3. Using the latest value of temperature, compute liquid and solid state solubility of silicon and the partition coefficient for each cell (Eqs.(13)-(15)).

4. For each of these cells, compare the latest concentration value and liquid solubility. If concentration exceeds the liquid solubility in one or more cells adjoining the seed crystal/solidified crystal, then solidification starts in these cells and proceed to step e for these solidifying cells.

5. Compute mass fraction solidified in this time step from the lever rule using Eq.$(10)_1$.

6. To prevent a cell from fully solidifying in one step, the actual mass fraction is computed from Eq.$(10)_2$.

7. Compute the cumulative sum of mass fraction solidified for each solidifying cell using Eq.$(10)_3$.

8. As soon as a cell becomes solidified completely (i.e. $\gamma = 1$) concentration in fully solidified cell is set to local solid-state solubility as per Eq.(14).

9. Update the thermal diffusivity and mass in the melt region using Eq. (9)

10. Compute the source terms from Eq.(8).

11. Solve energy and mass transport Eqs.(7).

12. Terminate computation when the desired simulation time is reached.

3.3   Boundary and Initial condition

3.3.1   Concentration field

The bottom and inner quartz walls are impermeable to transport of mass, which leads to a zero normal gradient boundary condition: $\partial C/\partial n = 0$. On the dissolution interface equilibrium is assumed and the concentration is prescribed as a function of temperature from the phase diagram. Liquidus and solidus curves were linearized for the temperature range of interest (1211.87-1289.37 K). It is important to note that these relations give the solubility in atomic percentage. In other relations, concentration is expressed in mass fraction.

$$C_l^{eq}(T) = 0.072075(T - 1211.87) \tag{12}$$

$$C_s^{eq}(T) = 0.336775(T - 1211.87) \tag{13}$$

$$K = (C_s^{eq}(T))/(C_l^{eq}(T)) \tag{14}$$

3.3.2   Thermal field

- Bottom: a constant temperature of 1176.87K was prescribed at the bottom.

- Outer quartz wall: a linear temperature gradient of 2.5K/mm was specified along the solution zone and a constant temperature of 1289.37K along the source.

- Top: radiative heat loss from the top was taken into account by using the following relation:

$$-\lambda \nabla T = \beta \sigma (T^4 - T_{amb}^4) \tag{15}$$

where $T_{amb} = 1284.37$K.

The OpenFOAM solver does not perform any computation at the axis of symmetry. Therefore, no boundary condition was specified along the symmetry axis. The concentration field was initialized to zero and the temperature field was initialized to 298K. The values of the physical properties used in the present work were obtained from Yildiz et al. (2005), Yildiz and Dost (2005), Slack and Glassbrenner (1960), Virzi (1991), Nakanishi et al (1999), and Yesilyurt et al. (1999).

4   Numerical Solution

To solve the field equations, a top-level code was written for OpenFOAM. Open-FOAM is based on the finite volume discretization technique. It uses a co-located, cell centered dependent variable storage arrangement. The mass diffusivity of silicon in solid germanium is several orders of magnitude smaller than that in molten germanium and the thermal diffusivity is different for the solid and liquid phases. Due to these factors, care must be taken while discretizing terms that involve these properties. For the melt region of the domain, mass and thermal diffusivities were defined as field variables and harmonic interpolation (Patankar (1980)) was used for discretizing the diffusion terms in the mass transport and energy equations. A constant time step of 2.0s was employed. The solution was considered converged when residuals had fallen below the specified solver tolerance of 10^{-9}. The release of latent heat and segregation of silicon from the melt into the solid crystal are incorporated in the numerical model by adding corresponding source terms in the field equations. The concentration in the growing crystal is governed by the solid-state solubility obtained from Eq.(14) utilizing the local temperature.

5   Results and Discussion

Figure 2 depicts the computed temperature and concentration fields in the melt and the shape of the initial growth interface after 1 hour of simulation time. The computed isotherms of the present simulation (shown on left in Fig.2) are relatively in a good agreement with those of Yildiz et al. (2005) and Yildiz and Dost (2005). This is due to the fact that the thermal field is not notably affected by the fluid flow in the melt. However, the computed iso-concentration lines (shown on right in Fig.2) show slight differences compared with the experiments of Yildiz et al. (2005) since we have not included the effect of fluid flow in the melt.

This difference is more prominent in the evolution of the growth interface that is shown in Fig.3. Although the total growth thickness for a 29h growth period is very close to those of the experiments of Yildiz et al (2005), the simulation predicts faster growth during the initial stages of growth as can be seen from Fig.3 and Table 2. The present simulation (on left in Fig.3) under zero gravity predicts faster initial growth (enhanced mass transport) compared with that of the Earth-bound experiments (in middle in Fig.3) in which while the mass transport in the upper section of the melt was mainly diffusion dominated, in the bottom region of the melt near the growth interface there were strong convective cells [Yildiz et al. (2005)]. For instance, as presented in Table 2, in the simulation of the Earth-bound experiments (middle) the growth thickness is about 6 mm at 10th growth hour while in the present simulation (left) the interface reaches the position of 8 mm during the same period. The experimental value is about 7 mm for this period.
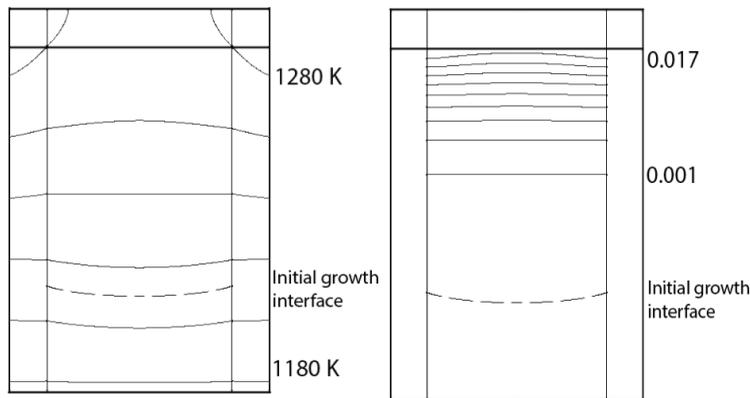

Figure 2: Computed isotherms (left), and iso-concentration lines (right) under zero gravity after 1h simulation time.

The observation of faster initial growth (enhanced mass transport) is contrary to commonly observed mass transport under the effect of natural convection, but agrees qualitatively with our experimental observations under a strong static magnetic field [Armour and Dost (2005a,b,c)]. As shown by Armour and Dost (2005a), in the Si-Ge system the application of a strong magnetic field does not suppress convection, but instead enhances mass transport in the solution. This observation was attributed to the nature of the Si-Ge system: namely in the absence of an applied magnetic field, lighter silicon diffuses from top into heavier germanium and transported by mainly diffusion in the upper region of the melt, however while heavier germanium at the bottom stabilizes system, strong convective cells develop near the
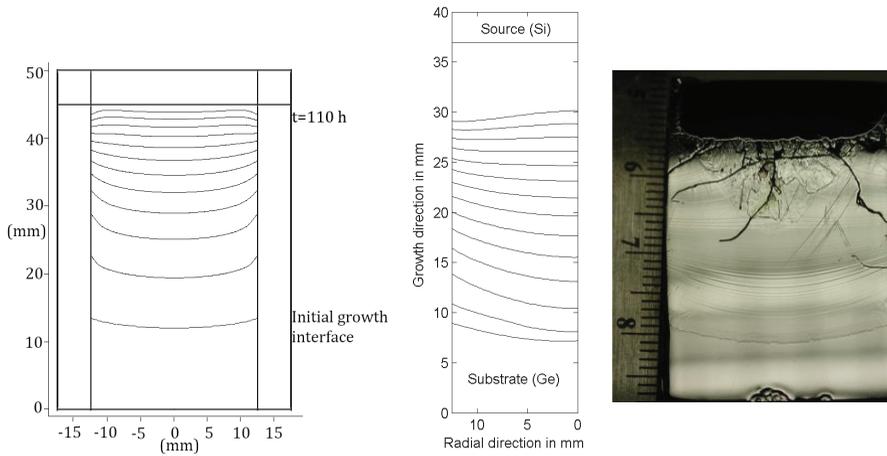
Figure 3: Computed evolution of the growth interface by the present simulation under zero gravity (on left, with time interval of 10h in between each line). The simulation including convection (after Yildiz et al. (2005) based on Earth-bound experiments (in middle, with time interval between each line is 3h (total of 39h growth), and only half zone is shown). As seen, simulation under zero gravity predicts slightly faster growth. Both simulations agree qualitatively with experiments of Yildiz et al. (2005) as seen from the striation lines of the sample on right (a total of 29h growth).

Table 1: Physical Properties [after Yildiz et a. (2005), Yildiz and Dost (2005), Slack and Glassbrenner (1960), Virzi (1991), Nakanishi et al. (1999), and Yesilyurt et al. (1999)].

Property	**Source** (Si)	**Seed** (Ge)	**Solution/Melt**	**Crystal** (Si_xGe_{1-x})	**Quartz**
λ (W/mK)	23.7	20.0	42.8	20.0	2.0
ρ (Kg/m^3)	2301.6	5323.0	5670.0	5323.0	2200.0
c_p	967.0	396.1	406.0	396.1	1200.0
D(m^2/s)	-	-	10^{-8}	-	-
β	0.71	-	-	-	0.85
L (kJ/kg)	-	466.5	466.5	-	-

Table 2: Comparison of growth thicknesses and interface evolution from Figure 3 (based on visual reading of the values after 29h growth).

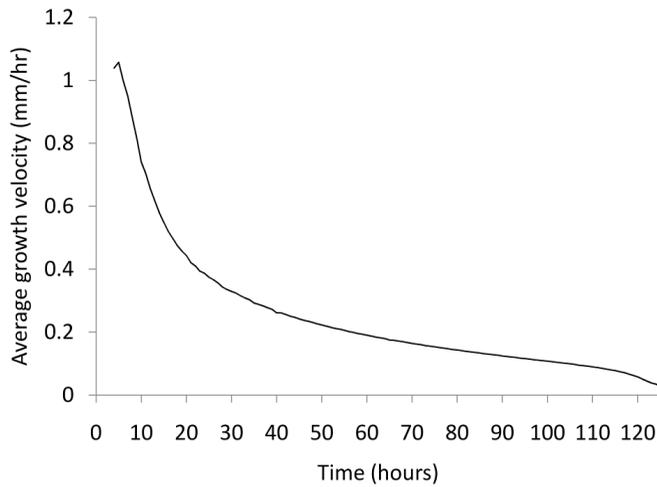|	**Present Simulation**	**Experiments of Yildiz et al. (2005)**	**Simulation of Yildiz et al. (2005)**
Total Growth Thickness (29h growth): centre	∼ 19 mm	∼ 19 mm	∼ 17 mm
Total Growth Thickness (29h growth): near wall	∼ 19 mm	∼ 16 mm	∼ 17 mm
Interface shape with respect to experiment	Flater at the centre, sharper near the wall		Sharper near the wall
Evolution of interface with respect to experiment	Faster near the wall		Better agreement with experiment
Growth thickness at centre after 10h growth	About 8 mm	About 7 mm	About 6 mm

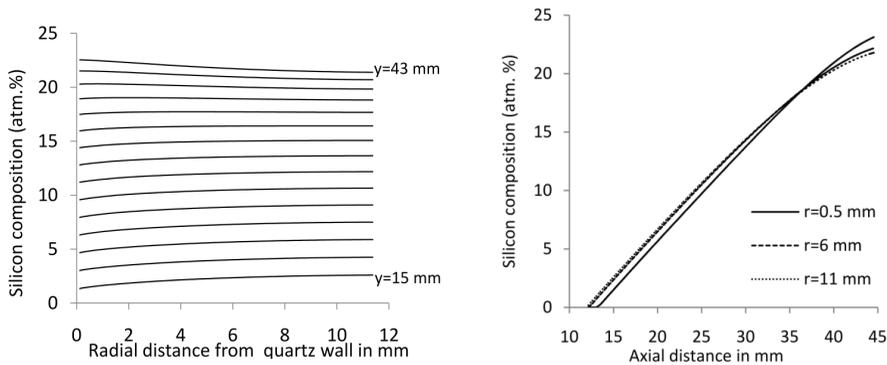Figure 4: Computed average growth velocity.

Figure 5: Computed radial (left) composition distribution and axial (right) composition profiles. Results agree qualitatively with the experimental results of Yildiz et al. (2005).

growth interface. The application of a strong magnetic field changes this balance by weakening the convective cells at the bottom and giving rise to the development of stronger convective cells in the upper region of the melt. Consequently, such a change in the flow structure of the melt leads to an enhanced mass transport in the melt.

Since there is no flow in the melt of the present simulation model, in the absence of strong convective cells in the melt, we predict faster initial growth and slightly different concentration distribution in the grown crystals. However, the evolution of the growth interface presents similar trend to that observed in experiments and also those from previous simulations, except that the flattening of the growth interface is delayed compared with that of experiments (as seen in Figure 3 on left in comparison with those in the middle and on right), and also growth initially faster along the crucible wall. The initial concave growth interface slowly flattens as growth progresses, and finally becomes convex near the end of the growth process similar to experiments.

The computed averaged growth velocity profile under zero gravity is given in Fig. 4. As predicted from experiments, the growth slows down as time progresses due to reduction in silicon dissolution into the growth melt since the melt is getting richer in silicon concentration and the concentration difference between the source and the melt is getting smaller.

Although we predict here a faster initial growth under zero gravity, the trend of the interface evolution and the total growth thickness after 29h growth agree with experiments. A well-designed LPD growth experiment (for SiGe) under microgravity

may shed light on these numerical predictions.

The computed axial and radial silicon composition profiles in the grown crystal are shown in Figure 5. As seen, these computed composition profiles are in qualitative agreement with the experimental results of Yildiz et al. (2005). Again, this implies that from a space experiment we may also expect a similar silicon distribution in the grown crystals; linear in the growth direction and almost uniform in the radial direction.

6   Summary

The fixed grid approach has been employed to model Liquid Phase Diffusion growth of SiGe under zero gravity. An integrated solver has been developed in Open-FOAM to simulate the process. The initial melting process is modeled using the well-known enthalpy method. This provides the necessary initial conditions for the subsequent solidification process, which is modeled using a virtual front tracking method. It was shown that the present simulation model that uses a fixed grid approach although agrees qualitatively with the experimentally observed interface evolution predicts a faster initial growth due to the absence of the contribution of gravity (fluid flow in the melt). The interface shapes are also slightly different and the flattening of the interface occurs later in time in comparison with that of the Earth-bound experiments. However, the temperature profiles in the LPD melt are in good agreement with those of the Earth-bound simulations as the thermal field is being less affected by fluid flow. The total growth thickness after 29h growth agrees with experiment.

Acknowledgement

References

Abrosimov, N. V.; Rossolenko, S. N.; Alex, V.; Gerhardt, A.; Schröder, W. (1996): Single crystal growth of $Si_{1-x}Ge_x$ by the Czochralski technique. *J. Crystal Growth*, vol. 166, pp. 657-662.

Abrosimov, N.V.; Rossolenko, S. N.; Thieme, W.; Gerhardt, A.; Schröder, W. (1997): Czochralski growth of Si- and Ge-rich SiGe single crystals. *J. Crystal Growth*, vol. 174, pp. 182-186.

Armour, N.; Dost, S. (2010a): Effect of a static magnetic field on silicon transport

in liquid phase diffusion growth of SiGe. *Crystal Research and Technology*, vol. 45, no. 3, pp. 244-248.

Armour, N.; Dost, S. (2010b): Silicon transport under rotating and combined magnetic fields in liquid phase diffusion growth of SiGe. *Crystal Research and Technology*, vol. 45, no. 4, pp. 335-340.

Armour, N.; Dost, S. (2010c): The Effect of Applied Magnetic Fields on Silicon Transport in Liquid Phase Diffusion Growth of SiGe. *ECS Transactions*, vol. 28, no. 5, pp. 161-170.

Bennon, W. D.; Incropera, F. P. (1987): A continuum model for momentum, heat and species transport in binary solid–liquid phase change systems-I. Model formulation. *Int. J. Heat Mass Transfer*, vol. 30, pp. 2161-2170.

Campbell, T. A.; Schweizer, M.; Dold, P.; Cröll, A.; Benz, K. W. (2001): Float zone growth and characterization of $Ge_{1-x}Si_x$ (x≤ 10 at%) single crystals. *J. Crystal Growth*, vol. 226, pp. 231-239.

Dold, P.; Barz, A.; Recha, S.; Pressel, K.; Franz, M.; Benz, K. W. (1998): Growth and characterization of $Ge_{1-x}Si_x$ (x≤10 at%) single crystals. *J. Crystal Growth*, vol. 192, pp. 125-135.

ElGanaoui, M.; Lamazouade, A.; Bontoux, P.; Morvan, D. (2002): Computational solution for fluid flow under solid/liquid phase change conditions. *Computers and Fluids*, vol. 31, pp. 539-556.

Fischer, B.; Friedrich, J.; Jung, T.; Hainke, M.; Dagner, J.; Fühner, T.; Schwesig, P. (2005): Modeling of industrial bulk crystal growth—state of the art and challenges. *J. Crystal Growth*, vol. 275, pp. 240-250.

Järvinen, J.; Nieminen, R.; Tiihonen, T. (1997): Time dependent simulation of Czochralski silicon crystal growth. *J. Crystal Growth*, vol. 180, pp. 468-476.

Kasper, E. (1995): Prospects of SiGeheterodevices. *J. Crystal Growth*, vol. 150, pp. 921-925.

Martínez-Tomás, C.; Muñoz, V. (2001): CdTe crystal growth process by the Bridgman method: numerical simulation. *J. Crystal Growth*, vol. 222, pp. 435-451.

Morvan, D.; El Ganaoui, M.; Bontoux, P. (1999): Numerical simulation of a 2D crystal growth problem in vertical Bridgman-Stockbarger furnace: latent heat effect and crystal-melt interface morphology. *Int. J. Heat Mass Transfer*, vol. 42, pp. 573-579.

Müller, G.; Friedrich, J. (2004): Challenges in modeling of bulk crystal growth. *J. Crystal Growth*, vol. 266, pp. 1-19.

Nakajima, K.; Kodama, S.; Miyashita, S.; Sazaki, G.; Hiyamizu, S. (1999):

Growth of Ge-rich Si_xGe_{1-x}single crystal with uniform composition (x=0.02) on a compositionally graded crystal for use as GaAs solar cells. *J. Crystal Growth*, vol. 205, pp. 270-276.

Nakajima, K.; Kusunoki, T. (1996): Constant temperature LEC growth of In-GaAs ternary bulk crystals using double crucible method. *J. Crystal Growth,* vol. 169, pp. 217-222.

Nakanishi,H.; Nakazato, K.; Abe, K.; Maeda, S.; Terashima, K. (1999):Temperature dependence of the density of molten germanium and silicon measured by a newly developed Archimedian technique. *J. Crystal Growth*, vol. 203, pp. 75-79.

Nikrityuk, P.; Pätzold, O.; Stelter, M. (2012): A fixed-grid method for transient simulations of dopant segregation in VGF-RMF growth. *J. Crystal Growth*, vol. 339, pp.75-85.

Okano, Y.; Umemura, S.; Dost, S.(2001): G-Jitter Effect on the Flow in a 3-Dimensional Rectangular Cavity. *J. Materials Processing and Manufacturing Sci.*, vol. 10, no. 1, pp. 3-6.

Okano, Y.; Shimizu, J.; Hayakawa, Y.; Hirata, A.; Dost, S. (2003): A Numerical Study for the Role Natural Convection in the Melting of a GaSb/InSb Sandwich System. *J. Num. Heat Transfer*, Part A, vol. 43, no. 1, pp. 31-46.

Okano, Y.; Ishii, A.; Miyashita, H.; Minakuchi, H.; Dost, S. (2006): A Numerical Study for Controlling the G-Jitter Induced Convection in the Solution of a Crystal Growth Crucible under Microgravity. *J. Fluid Dynamics and Materials Processing (FDMP)*, vol. 2, no. 4, pp. 261-269.

OpenCFD (2013): OpenFOAM: The Open Source CFD Toolbox, http://www.open foam.com.

Ouyang, H.; Shyy, W. (1996): Multi-zone simulation of the Bridgman growth process of β-NiAl crystal. *Int. J. Heat Mass Transfer*, vol. 39, no. 10, pp. 2039-2051.

Ouyang, H.; Shyy, W. (1997): Numerical simulation of CdTe vertical Bridgman growth. *J. Crystal Growth*, vol. 173, pp. 352-366.

Patankar, S.V. (1980): *Numerical Heat Transfer and Fluid Flow,* first ed., Hemisphere, New York.

Schilz, J.; Romanenko, V. N. (1995): Bulk growth of silicon-germanium solid solutions. *J. Mater. Sci. Mater. Electron,* vol. 6, pp. 265-279.

Shyy, W.; Udaykumar, H. S.; Rao, M. M.; Smith, R. W. (1996): *Computational Fluid Dynamics with Moving Boundaries*, first ed., Taylor &Francis, London.

Slack, G.A.; Glassbrenner, C. (1960): Thermal conductivity of germanium from 3˚K to 1020˚K. *Phys. Rev.*, vol. 120 , pp. 782-789.

Suzuki, T.; Nakajima, K.; Kusunoki, T.; Katoh, T. (1996): Multicomponent Zone Melting Growth of Ternary InGaAs Bulk crystal. *J. Electron. Mater.* vol. 25, pp. 357-361.

Takagi, Y.; Suzuki, N.; Okano, Y.; Tanaka, A.; Hayakawa, Y.; Dost, S. (2012): Numerical Simulation of the Dissolution Process of GaSb into InSb Melt under Normal and Microgravity Conditions. *Trans. ISASS* (The Japanese Society of Aeronautical and Space Sciences), vol. 10, no. 28, pp. 1-7.

Usami, N. (2011): Types of silicon-germanium (SiGe) Bulk Crystal Growth Methods and Their Applications, in : Y. Shiraki and N. Usami (Eds), Silicon-Germanium (SiGe) Nanostructures-Production, Properties and Applications in Electronics, Woodhead Publishing, Cambridge, pp. 72-82.

Van den Bogaert, N.; Dupret, F. (1997): Dynamic global simulation of the Czochralski process I. Principles of the method. *J. Crystal Growth,* vol. 171, pp. 65-76.

Virzi, A. (1991): Computer modelling of heat transfer in Czochralski silicon crystal growth. *J. Crystal Growth*, vol. 112, pp. 699-722.

Voller, V. R.; Prakash, C. (1987): A fixed grid numerical modeling methodology for convection-diffusion mushy region phase-change problems. *Int. J. Heat Mass Transfer*, vol. 30, pp. 1709-1720.

Volz, M. P.; Schweizer, M.; Kaiser, N.; Cobb, S. D.; Vujisic, L.; Motakef, S.; Szofran, F. R. (2002): Bridgman growth of detached GeSi crystals. *J. Crystal Growth*, vol. 237-239, pp. 1844-1848.

Weller, H.G.; Tabor, G.; Jasak, H.; Fureby, C. (1998): A tensorial approach to computational continuum mechanics using object-oriented techniques. *Computers in Physics*, vol. 12, no. 6, pp. 620-631.

Wollweber, J.; Schulz, D.; Schröder, W. (1996a): Extremely reduced dislocation density in Si_xGe_{1-x} single crystals grown by the float zone technique. *J. Crystal Growth*, vol. 158, pp. 166–168.

Wollweber, J.; Schulz, D.; Schröder, W. (1996b): Si_xGe_{1-x} single crystals grown by the RF-heated float zone technique. *J. Crystal Growth*, vol. 163, pp. 243–248.

Yeckel, A.; Derby, J. J. (2005): Computer Modelling of Bulk Crystal Growth, in: P. Capper (Ed.), Bulk Crystal Growth of Electronic, Optical and Optoelectronic Materials, John Wiley and Sons, New York, pp. 73-113.

Yesilyurt, S.; Vujisic, L.; Motakef, S.; Szofran, F. R.; Volz, M. P. (1999): A numerical investigation of the effect of thermoelectromagnetic convection (TEMC) on the Bridgman growth of $Ge_{1-x}Si_x$. *J. Crystal Growth,* vol. 207, pp. 278–291.

Yildiz, E.; Dost, S. (2007): A numerical simulation study for the combined effect of static and rotating magnetic fields in liquid phase diffusion growth of SiGe. *J.*

Crystal Growth, vol. 303, pp. 279-283.

Yildiz, E.; Dost, S.; Yildiz, M. (2006): A numerical simulation study for the effect of magnetic fields in liquid phase diffusion growth of SiGe single crystals. *J. Crystal Growth*, vol. 291, pp. 497-511.

Yildiz, M.; Dost, S.; Lent, B. (2005): Growth of bulk SiGe single crystals by liquid phase diffusion. *J. Crystal Growth,* vol. 280, pp. 151-160.

Yildiz, M.; Dost, S. (2005): A continuum model for the Liquid Phase Diffusion growth of bulk SiGe single crystals. *Int. J. Eng. Sci.,* vol. 43, pp. 1059-1080.

Yonenaga, I.; Matsui, A.; Tozawa, S.; Sumino, K.; Fukuda, T. (1995): Czochralski Growth of $Ge_{1-x}Si_x$ alloy crystals. *J. Crystal Growth*, vol. 154, pp. 275-279.

Yonenaga, I. (2005): Growth and fundamental properties of SiGe bulk crystals. *J. Crystal Growth*, vol. 275, pp. 91-98.

Zhu, M.F.; Stefanescu, D. M. (2007): Virtual front tracking model for the quantitative modeling of dendritic growth in solidification of alloys. *Acta Materialia*, vol. 55, pp. 1741-1755.

Nomenclature

C_p	specific heat
C	mass fraction
D	diffusion coefficient
H	enthalpy
K	partition coefficient
L	latent heat
S_c	source term in the mass transport equation
S_t	source term in the energy equation for melting
S'_t	source term in the energy equation for solidification
t	time
T	temperature

Subscripts

amb	ambient
l	liquid phase
p	control volume
s	solid phase

Superscripts

eq	equilibrium
n	time step
N	number of time steps after solidification starts in a given cell
N_T	total number of time steps in which a cell completely solidifies after it is captured as a solidifying cell

Greek symbols

α	thermal diffusivity
β	emissivity
ε	liquid fraction
$\Delta\gamma$	mass fraction solidified in one time step
$\Delta\gamma_{lever}$	mass fraction solidified in one time step as per lever rule
γ	cumulative sum of mass fraction solidified in a given cell
λ	thermal conductivity
σ	Stefan-Boltzmann constant